

L. K. Mansur, Metals and Ceramics Division, Oak Ridge National Laboratory, P.O. Box 2008,  
Oak Ridge, TN 37831-6376, USA

**ABSTRACT:** Development of structural materials to withstand aggressive radiation environments has been carried out on an international scale over the past four decades. Major radiation-induced changes in properties include swelling, creep and embrittlement. The basic work, stimulated by technology, to understand and control these phenomena, has been heavily oriented toward the evolution of microstructures and their effects on properties. Microstructural research has coupled analyses by high resolution techniques with theoretical modeling to describe and predict microscopic features and the resulting macroscopic properties. A short summary is presented of key physical considerations that drive these changes during irradiation. Such processes begin with displacement cascades, and lead to property changes through the diffusion and clustering of defects. Examples of radiation effects in two different systems of recent interest are highlighted--the vessel of a research reactor, and target materials in a high powered accelerator spallation source.

## 1. INTRODUCTION

The wholesale creation of microstructures in materials by particle irradiation is by now a well known phenomenon. A rich variety of features is found ranging from small three-dimensional clusters and dislocation loops to dislocation networks, cavities and second phase precipitates, for example. Work in this field has been carried out over the last four decades. It is therefore not realistic to attempt to represent even a small part of the field in a single short paper. In the present contribution, several concepts are summarized that have proven key to understanding the origins and development of radiation effects in materials.

References to more complete descriptions are provided for the interested reader. References [1] and [2] contain reviews of the methods of reaction rate theory used to model microstructural development, together with substantial supporting reviews of experimental background. Reference [3] reviews the field from a different perspective. The proceedings of an international summer school on radiation effects includes a number of relatively comprehensive papers on subtopics of the field [4]. Finally, several conference series [5,6] document the sustained long term efforts and evolution in the area, including many papers on practical applications of the more basic studies.

In these works the remarkable variety and detail of microstructures produced by irradiation, and their dependence on material composition are well described. However, equally important are the effects of different irradiation environments on properties, brought about by changes in microstructures. This is the emphasis in the present paper. After developing an essential background in the next section, two examples of quite different irradiation conditions of recent and future interest are described.

## 2. BACKGROUND

When a material is irradiated, virtually every property may change. This includes physical dimensions, as well as mechanical, electrical, magnetic, optical and other properties. The reason for this is that the existing crystal and defect structure is deconstructed and reconstructed on an atom by atom basis during irradiation. In a high dose irradiation, each atom may be displaced from its lattice site tens or hundreds of times. The standard measure of radiation dose in metallic materials is the displacement per atom (dpa). Conditions during irradiation such as temperatures, dose rate, dose and local alloy composition determine property changes that will ultimately result.

\*Research sponsored by the Division of Materials Sciences, U.S. Department of Energy under contract number DE-AC05-96OR22464 with Lockheed Martin Energy Research Corporation.

**DISCLAIMER**

**Portions of this document may be illegible  
in electronic image products. Images are  
produced from the best available original  
document.**

## **DISCLAIMER**

This report was prepared as an account of work sponsored by an agency of the United States Government. Neither the United States Government nor any agency thereof, nor any of their employees, makes any warranty, express or implied, or assumes any legal liability or responsibility for the accuracy, completeness, or usefulness of any information, apparatus, product, or process disclosed, or represents that its use would not infringe privately owned rights. Reference herein to any specific commercial product, process, or service by trade name, trademark, manufacturer, or otherwise does not necessarily constitute or imply its endorsement, recommendation, or favoring by the United States Government or any agency thereof. The views and opinions of authors expressed herein do not necessarily state or reflect those of the United States Government or any agency thereof.

Figure 1 shows the time (left) and energy (right) scales that apply during a typical neutron irradiation. The cascade of displaced atoms and vacant lattice sites is essentially complete in  $10^{-13}$  s. As a result of this event, the matrix will be in an unstable state where defects may recombine, cluster and undergo rearrangements. Interstitial and vacancy diffusion occur on longer time scales. The development of microstructure occurs over time scales up to 19 or 20 orders of magnitude longer than the initial transfers of kinetic energy in the cascade. The energy scale has a wide span as well. The typical fast neutron in a reactor is at an energy of about 1 MeV. However, defect diffusion occurs at thermal energies, i.e., hundredths of eV.

Figure 2 is a pictorial representation of molecular dynamics simulation [7] of a cascade at 100 K in iron, 200 ps after an energy of 20 keV was imparted to one of the atoms (the primary knock-on atom or pka). This energy corresponds to the maximum energy transfer possible from a neutron of energy approximately 280 keV. The long term development of microstructure is well represented in the transmission electron micrograph (TEM) of Figure 3 [8]. It shows dislocation network, dislocation loops, cavities and second phase precipitates. None of the microstructures visible there would be observed on this scale prior to irradiation. The results are for a 316 type stainless steel irradiated in the EBR-II reactor to a fluence of  $1.9 \times 10^{26}$  n/m<sup>2</sup> (about 10 dpa) at 580°C [8]. Extensive microstructural characterization work of this type has been carried out over many years to permit the rather thorough characterization of radiation response with dose and temperature, for example, of many structural materials.

Figure 4 is a flow chart showing the creation of point defects by displacements, and the various paths for their disposition. They may cluster to form extended defects, or be absorbed at existing or newly created sinks. On this path (left) the defects may contribute to the buildup of microstructure and to property changes. On the other path (right), self-interstitials and vacancies may recombine at various locations producing no long term property changes. Figure 4 also conveniently represents the theoretical framework that has been developed to understand radiation effects in structural materials. Essentially, each entry represents a subfield of theory or modeling effort. The terms at the bottom left: swelling, creep, and embrittlement are effects of radiation that have occupied the lion's share of the efforts of people working in this field. A series of articles for the nonspecialist on the theoretical and computational aspects of radiation effects in materials is contained in a very recent issue of JOM (formerly, Journal of Metals) [9].

Swelling is the isotropic volume expansion of an irradiated material. It occurs by the net absorption of interstitials at dislocations, with a corresponding net number of vacancies accumulating at cavities. It may reach tens of percent or more at high doses, e.g., tens to hundreds of dpa. The proximate cause of swelling is the asymmetrical partitioning of defects between cavities on the one hand, and other sinks on the other hand. The main "other" sink is usually dislocations, including dislocation loops, although precipitates, grain boundaries, and free surfaces can be important under certain conditions. The dominant processes responsible for this asymmetrical partitioning of interstitials to dislocations and vacancies to cavities depend upon the material and irradiation conditions: interstitials may be stored in interstitial dislocation loops and vacancies in cavities; dislocations and cavities may have different capture efficiencies for interstitials and vacancies, because of elastic and diffusional interactions; interstitials and vacancies may be produced in different clustering fractions in cascades and may, then, decay thermally or be swept up by dislocations differently; other partitioning processes may also contribute. Swelling has received a great deal of experimental and theoretical attention. As a result, a certain measure of understanding of the phenomenon has been achieved. It is now possible to design swelling-resistant alloys based on the combined results of theoretical modeling and a series of critical experiments [2].

Irradiation creep is a shape change in compliance with an applied stress, in excess of ordinary thermal creep. It occurs even at quite low temperatures, where thermal creep is entirely negligible. Dislocation climb creep occurs by the asymmetrical partitioning of self-interstitials and vacancies to dislocations differently oriented to the stress axis. Climb-enabled glide creep occurs when a dislocation climbs and overcomes an obstacle, permitting it to glide. Creep may therefore result directly from net climb of particularly oriented dislocations, or indirectly from any climb that triggers glide in response to the applied stress.

Embrittlement occurs broadly speaking, by two processes. In the first type of process, hardening of the material progresses by creation of many types of obstacles by radiation. This hardening reduces ductility. Some of the obstacles are shown in Figure 3. However, many of the most effective

hardening centers are very small and would not appear visible by TEM. Atom probe field-ion microscopy has contributed much of the knowledge of the structure and properties of these very fine hardening features [10,11]. The second type of process is grain boundary weakening caused both by transmutation products, such as helium, and by changes such as radiation-induced segregation (RIS) in composition near the grain boundary. Both of the examples of current research topics, which make up the remainder of this paper, mainly concern embrittlement. Both examples emphasize current and future research, and indicate how more basic investigations on property changes support technology applications. The examples cited cover recent work on light water fission reactor vessel materials, and needed future work on container materials for spallation neutron sources.

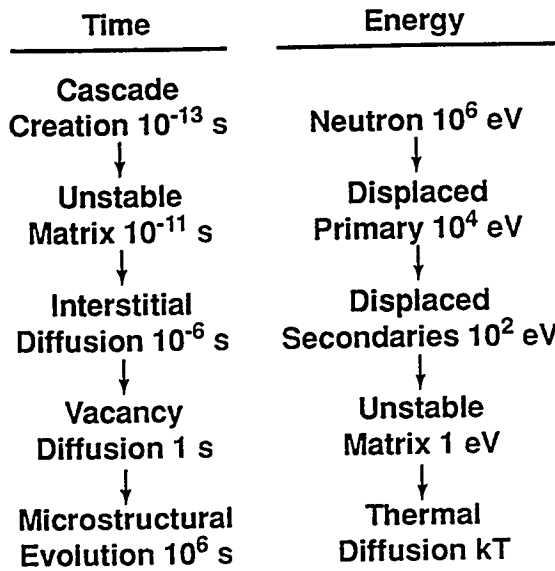


Fig. 1. Time and energy scales for processes caused by displacement of atoms leading to changes in microstructure.

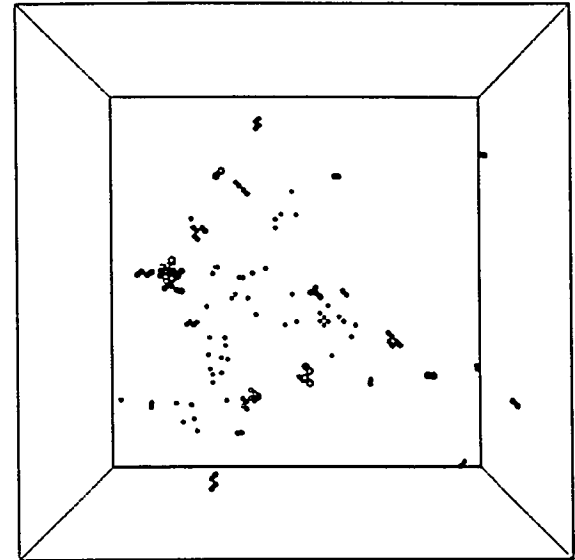


Fig. 2. Defects remaining 200 ps after the initiation of a 20 keV molecular dynamics simulation. The box is 14 nm on a side; black dots are vacancies; larger gray symbols are interstitials.



Fig. 3. Microstructure of high purity 316 stainless steel neutron irradiated at  $580^{\circ}\text{C}$  to a dose of  $1.9 \times 10^{26}$  n/m<sup>2</sup>.

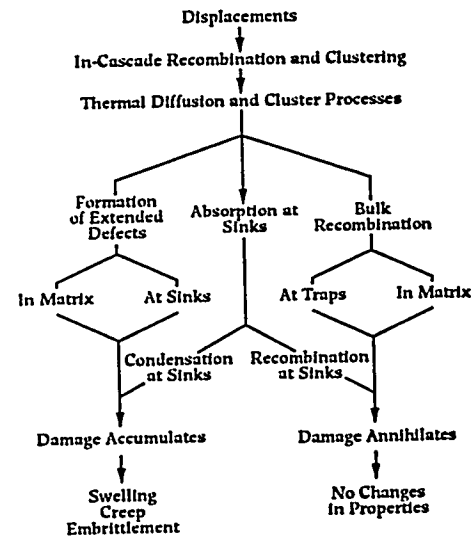


Fig. 4. Flow diagram showing various fates of point defects after they are created by irradiation.

### 3. EMBRITTLEMENT OF THE HFIR REACTOR VESSEL

The High Flux Isotope Reactor (HFIR) at Oak Ridge National Laboratory is a high-flux mixed-spectrum multipurpose reactor. It is used for research in neutron scattering, in materials irradiation and

in the production of isotopes. In 1986 it was found that the reactor vessel material was becoming embrittled at a more rapid rate than expected [12,13]. In that work, Charpy impact data from the HFIR surveillance program indicated that embrittlement was occurring at fast neutron fluences five to ten times lower than expected. These findings of "accelerated" or "early" embrittlement were based on extrapolations of data obtained in test reactors at in-core or near-core positions under fast-spectrum, high-damage-rate conditions. Figure 5 summarizes this embrittlement situation. The test reactor data, accumulated at fast neutron fluences ( $E > 1 \text{ MeV}$ ) above about  $2 \times 10^{22} \text{ n/m}^2$  indicate that no embrittlement (as measured by increase in Charpy transition temperature) should be expected when extrapolated downward for fluences below about  $6 \times 10^{21} \text{ n/m}^2$ . However, measurements on Charpy impact specimens irradiated near the HFIR pressure vessel at fluences as low as  $1 \times 10^{21} \text{ n/m}^2$  indicated upward shifts in the ductile-to-brittle transition temperature of tens of °C.

Several mechanisms to explain this discrepancy were explored. These included the possibility of thermal aging-induced hardening over an approximately 20 year period; enhanced availabilities of point defects to induce clustering and precipitation, either (or both) because of an extremely low damage rate or because of a thermalized neutron spectrum; increased damage from the boron ( $n, \alpha$ ) reaction; and an effect of copper precipitation on hardening [14]. Each of these possibilities was examined by experiments and/or analysis, and each was ruled out.

It is now clear [14,15] that the "accelerated" embrittlement of the HFIR vessel is due to uncounted displacements caused by  $\gamma$ -rays. The cause was uncovered in the following way. Because of the unusual embrittlement results and the need to confirm detailed particle transport calculations for regions near the vessel, it was decided to carry out extensive dosimetry at several locations at the HFIR vessel. In the dosimetry experiments, significant discrepancies were found between  $^9\text{Be}$  and  $^{237}\text{Np}$  monitors, on the one hand, and Ni monitors on the other hand. The former indicated apparent fast neutron fluxes about 15 times those indicated by the latter. The discrepancy between these monitors and the Ni monitors was explained when it was realized that the excess reaction products of the Be and Np monitors were accounted for by photonuclear events. The Be and Np monitors undergo photonuclear reactions, ( $\gamma, n$ ) for the former and ( $\gamma, \text{fission}$ ) for the latter. These augment the fast neutron reactions in creating reaction products that are measured in the dosimetry experiments. These results were confirmed by additional dosimetry and by transport calculations, which showed that,  $\phi_\gamma / \phi_n \sim 10^4$  HFIR vessel. Here  $\phi_\gamma$  and  $\phi_n$  indicate the hard gamma ray flux  $\geq 2 \text{ MeV}$  and the fast neutron flux  $\geq 1 \text{ MeV}$ , respectively. Recent analyses, however, have shown that the atomic displacement cross-section for  $\gamma$ -rays in the energy range appropriate to the HFIR is of order 1 barn, while the displacement cross-section for fast neutrons is of order 1,000 barn [16,17]. Thus, the ratio of  $\phi_\gamma / \phi_n$  above shows immediately that hard  $\gamma$ -rays produce most of the displacements in the HFIR vessel. The reason for the high ratio can be seen in Figure 6. The figure shows the attenuation of both neutron and gamma fluxes

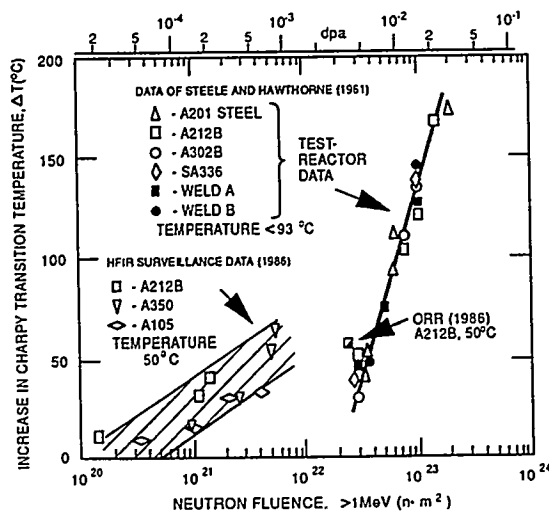


Fig. 5. Charpy transition temperatures in various pressure vessel steels plotted against fast neutron fluence.

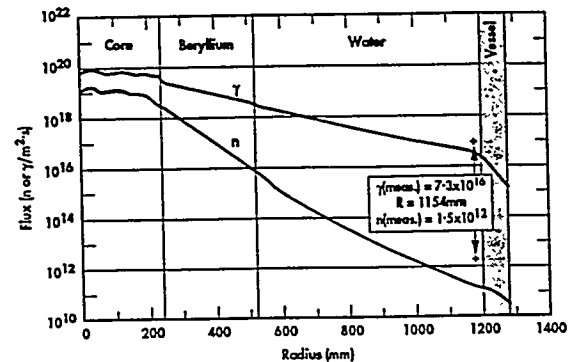


Fig. 6. Fast neutron and hard gamma flux as functions of distance from the center of the HFIR reactor core.

with distance from the core (fuel, Al structure and Be reflector) [18]. It can be seen that the neutrons are attenuated much more effectively than the  $\gamma$ -rays by the water surrounding the core. In the core the gamma flux exceeds the fast neutron flux by only severalfold. At the vessel the ratio is about  $10^4$ .

When the additional displacements produced by the  $\gamma$ -rays are accounted for, the apparent discrepancy of Figure 5 is removed. When the  $\gamma$ -displacements are included, the data points in the shaded band for the HFIR are translated so that they fall on the same line as the points for the test reactor data. The latter were obtained at in-core and near-core positions. The implications of this work are that in reactors with large water paths, the components so exposed may be subject to  $\gamma$ -embrittlement. Fortunately,  $\gamma$ -induced displacements are not expected to be significant with respect to fast neutron displacements in most existing water-cooled reactor vessels, because the water gaps are not sufficiently large [19].

#### 4. RADIATION EFFECTS IN MATERIALS FOR SPALLATION NEUTRON SOURCES

An entirely different application, where radiation-induced changes in microstructure may cause significant changes in properties, concerns particle accelerators. In particular, targets in high-power accelerators optimized to produce spallation neutrons will present challenges for materials scientists. Spallation refers to the processes triggered when high energy particles, typically protons of order 1 GeV, impinge on nuclei. Neutrons are released as the energy of the interaction is dissipated. Typically 20 to 30 neutrons are released for each proton impinging on the target. Target materials of choice are heavy nuclei containing many neutrons; candidates include solid materials such as Ta and W, and liquid metals such as Hg and Pb-Bi eutectic. Research facilities have been proposed as neutron sources for neutron scattering and materials irradiation research. Proposals have also been made for the construction of accelerator plants for the transmutation of nuclear waste and for the production of various isotopes species such as tritium or medical isotopes, for example.

Recently, there has been a great deal of interest in spallation neutron sources for neutron scattering. Several facilities are now in conceptual design. The European Spallation Source, the Japanese Neutron Science Research Center, and the National Spallation Neutron Source (NSNS) in the United States, in particular, plan to use liquid Hg targets for the production of neutrons. Although the liquid Hg target does not suffer radiation damage in the same sense as solid materials, the target container materials and associated structures will experience severe radiation damage. Materials issues associated with spallation targets of this type were examined at a recent workshop [20].

Figure 7 is an artist's rendition of the planned NSNS, showing the stainless steel container for the Hg target in relation to the incident proton beam and other structures. The container will be subject to the most severe irradiation. The front region of the container will be subject to incident protons in the 1-2 GeV range. The target container will also be subject to neutrons ranging in energy from the proton energy down to thermal energies. For the initial power level of 1 MW for the NSNS, the damage rate at the container face is expected to be about 32 dpa/yr. Both the presence of the protons, whose damage and transmutation cross-sections are similar to those of neutrons above several tens of MeV, and the high energy portion of the neutron spectrum, make the spallation environment unusual in terms of most previous experience in materials irradiation. In fission reactors, there are very few neutrons above 10 MeV, with most below 1 MeV. In fusion reactors, now under research and development as a power source for the 21st century [6], the neutrons are below about 14 MeV. Figure 8 shows the shape of the neutron spectrum for the NSNS, with a  $^{235}\text{U}$  fission spectrum superimposed for comparison [21].

The difference in spectrum shown in Figure 8 means that materials in the spallation environment will be subject to different displacement characteristics and transmutation cross-sections. Figure 9 shows the displacement cross-sections in 316 stainless steel and tungsten, an alternate target material to mercury, as a function of energy [22]. In stainless steel, the displacement cross-section does not increase strongly in the MeV to GeV range. However, the maximum kinetic energy imparted to a primary knock-on atom by a neutron or proton as a fraction of the neutron energy varies as  $4(m_n m_A)/(m_n + m_A)^2$ , where  $m_n$  is the neutron mass and  $m_A$  is the atomic mass of the struck atom. Thus, for stainless steel the maximum energy of the primary knock-on atom is  $\sim 1/15$  the projectile energy, or 67 keV for a 1 MeV neutron versus 67 MeV for a 1 GeV neutron or proton. Qualitatively, the high energy pka is like bombarding the material with ions in the MeV range. Cascades produced

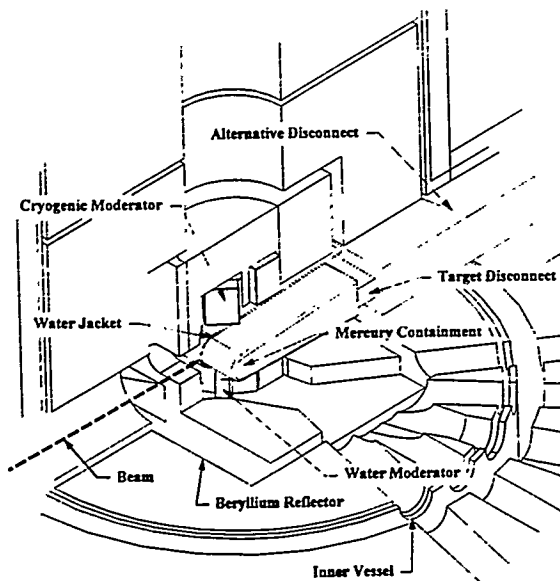


Fig. 7. Pictorial representation of the NSNS target region.

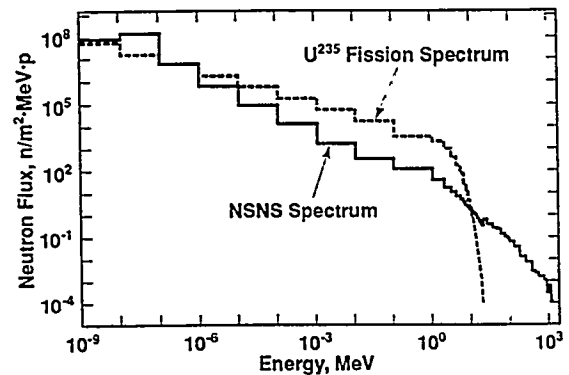


Fig. 8. Neutron spectrum for the NSNS front target. Also, shown is a  $^{235}\text{U}$  fission spectrum normalized to the same height at the lowest energy.

by very high energy pka's are known to break up into subcascades whose characteristics are similar to cascades produced by pka's in the range 30-50 keV. Nevertheless, some differences may be expected that may influence microstructural development. The most obvious is that even if a pka of, say, 10 MeV energy produced 200 subcascades, each of identical characteristics as a cascade of 50 keV, the subcascades from the high energy event would be produced with a very strong time and space correlation. The same number of 50 keV cascades from the low energy irradiation would be produced randomly in space and time. Thus, even if the average damage rates of the two irradiations were identical, differences in cluster nucleation and survival could result.

A second, less subtle, type of difference lies in transmutation rates. Figure 10 shows expected helium transmutation rates in fission, fusion and spallation environments. Helium is an insoluble inert gas that can cause or exacerbate grain boundary embrittlement and trigger swelling. Fast fission reactors produce helium in materials like steels at rates of a few tenths appm/dpa. Fusion reactors, which are normally thought of as high helium producers, yield helium at about 10 appm/dpa. The spallation environment, however, will yield helium at more than an order of magnitude higher than this rate, up to about 200 appm/dpa for stainless steels. Helium at these levels can contribute to hardening and hardening-associated embrittlement at low temperatures. At high temperatures such levels of helium can cause extreme grain boundary embrittlement. Also shown in Figure 10 is a special case encountered in mixed spectrum reactors. The two step thermal neutron reaction,  $^{58}\text{Ni}(n,\gamma)^{59}\text{Ni}(n,\alpha)^{56}\text{Fe}$ , proceeds with relatively high cross-sections, resulting in the amount of helium as a function of dose shown. This amount approaches half that expected in the spallation environment at high doses. Thus, mixed spectrum fission reactor irradiations can be utilized to provide relevant information on the effects of He on stainless steels irradiated in a spallation environment. In the NSNS, it has been calculated that the damage accumulation rate would be  $\sim 32$  dpa/year for the initial 1 MW power level at the peak beam position on the front of the target, and  $\sim 160$  dpa/year for the 5 MW second phase upgrade. These damage rates,  $\sim 10^{-6}$  dpa/s, are in the same range, on average, as for the core regions of high flux reactors and of future fusion reactors.

In addition, the NSNS and similar facilities are expected to operate in a pulsed mode. The pulse structure will consist of pulses of order 1  $\mu\text{s}$ , separated by beam-off intervals of order 20 ms. The power levels quoted in the previous paragraph are average levels. During a pulse, the instantaneous power will be a factor of about  $10^4$  larger, and the damage rate  $\sim 10^{-2}$  dpa/s. In addition to differences in microstructure caused by differences in instantaneous damage rates, the on-off cycle changes the kinetics of point defect buildup, which may result in changes in the accumulation of extended defect microstructure, such as dislocation loops and other types of clusters. These changes may, therefore, result in different mechanical properties than in steady irradiations. Some data is available from pulsed irradiations using ion accelerators [23]. In that work it was found that pulsing at different pulse intervals caused changes in the sizes of dislocation loops, which would be expected to lead to changes

in mechanical properties in a bulk specimen. These results were consistent with theoretical predictions for the effects of pulsing. New work in this area would be of value both to fundamental understanding and to the technology of target materials for spallation accelerators.

In addition to helium, other transmutation products will be produced at unusually high levels in spallation target materials. These include hydrogen and other heavier species. The calculated hydrogen production rate in stainless steel is about a factor of 10 higher than He. H is of concern, especially in the presence of He, since it may become trapped as  $H_2$  in He bubbles or other clusters and contribute to embrittlement. The production of solid transmutation products at high incident proton or neutron energies is also substantially higher than in fission reactors. The production peaks near the atomic number of the parent species and has a tail down to significantly lower numbers.

We may summarize the discussion in this section to say that spallation irradiation conditions are unusual in terms of previous experience. Some experimental data are available from spallation environments, however, it is generally at low dose; for some important materials, is either sparse or even non-existent. Similarly, theory and modeling of radiation effects has been very little applied to spallation irradiation conditions. This offers great opportunities for new work on the microstructural responses to this unique irradiation environment.

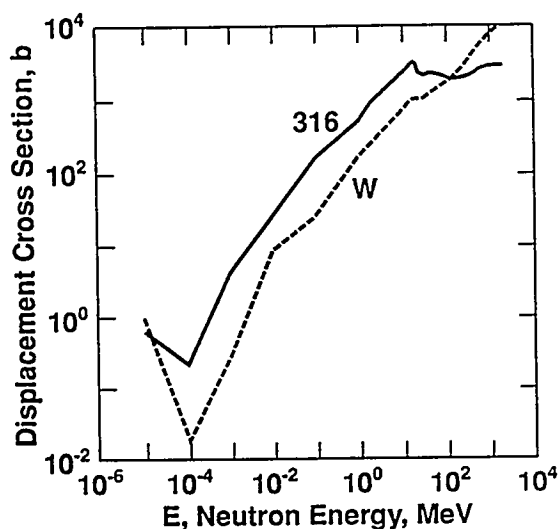


Fig. 9. Calculated displacement cross-sections for 316 stainless steel and tungsten, as a function of energy.

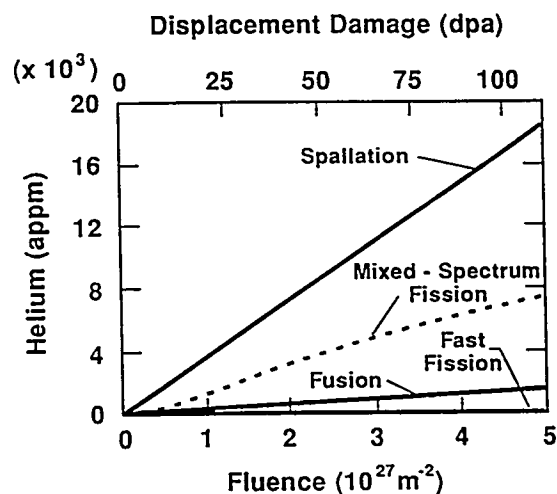


Fig. 10. Calculated accumulation of helium with dose for 316 stainless steel in several irradiation environments.

## 5. SUMMARY

In the field of radiation materials science, most of the activity has been devoted to the dual questions of how irradiation produces changes in microstructures, and how properties are changed in response to the evolving microstructures. Much of the literature consists of characterization studies of the detailed microstructural response of materials to irradiation based on variations in materials parameters. Equally important work has emphasized the role of the irradiation environment on the microstructural development and macroscopic property changes.

The present paper highlights key concepts developed to understand how irradiation produces these changes. Two examples of the effects of irradiation environment on materials are then described. By this approach it is intended to give a flavor of very recent and future work in the field, and at the same time introduce the connection of the more basic research with technological applications and engineering systems. The first example describes current and recently completed research on the  $\gamma$ -embrittlement of a reactor pressure vessel. In the second example, where more research will be concentrated in the future, the spallation radiation damage environment of target materials in high powered accelerators is highlighted. In both cases and for radiation effects in materials in general, there is the continuing need to understand how the changes in microstructure and composition caused by irradiation dictate macroscopic property changes.

## References

- [1] L. K. Mansur, "Mechanisms and Kinetics of Radiation Effects in Metals and Alloys," A chapter in the book, *Kinetics of Non-Homogenous Processes*, edited by G. R. Freeman, Wiley-Interscience, New York 1987, pp. 377-463.
- [2] L. K. Mansur, *J. Nucl. Mater.* **216** (1994) 97-123.
- [3] W. Schilling and H. Ullmaier, "Physics of Radiation Damage in Metals," Materials Science and Technology, R. W. Cahn, P. Haasen and E. J. Krammer, eds., v. 10B, pp. 179-241, 1995, VCH Publisher, Weinheim, Germany.
- [4] Proceedings of the International Summer School on the Fundamentals of Radiation Damage, I. M. Robertson, R. S. Averback, D. K. Tappin and L. E. Rehn, eds., *J. Nucl. Mater.* **216** (1994) 1-368.
- [5] See the proceedings of the biennial series on Effects of Radiation on Materials of the American Society of Testing and Materials. The latest publications in this series are: 17th Symposium, ASTM STP 1270, 1996; 16th Symposium, ASTM STP 1175, 1994; ASTM STP 1125, 1992.
- [6] See the proceedings of the series of International Conferences on Fusion Reactor Materials published in the Journal of Nuclear Materials. The latest publications in this series are: ICFRM-7, (in press); ICFRM-6, **212-215** (1994) 1-1082; ICFRM-5, **191-194** (1992) 1-1506.
- [7] R. E. Stoller, "Point Defect Survival and Clustering Fractions Obtained from Molecular Dynamics Simulations of High Energy Cascades," *J. Nucl. Mater.* (in press).
- [8] J. O. Stiegler and L. K. Mansur, *Ann. Rev. Mater. Sci.* **9** (1979) 405-454.
- [9] See the series of four articles on modeling of radiation effects by R. E. Stoller, H. L. Heinisch, E. P. Simonen, and L. K. Mansur in *JOM*, a publication of the Minerals, Metals and Materials Society, December, 1996 (in press).
- [10] M. K. Miller, "Atomic Level Microstructural Characterization by APFIM," these proceedings.
- [11] G.D.W. Smith, *et al.* "Three Dimensional Atom Probe Microanalysis," these proceedings.
- [12] R. K. Nanstad, S. K. Iskander, A. F. Rowcliffe, W. R. Corwin, and G. R. Odette, "Effects of 50°C Surveillance and Test Reactor Irradiations on Ferritic Pressure Vessel Steel Embrittlement," *Effects of Radiation on Materials: 14th International Symposium (Volume II)*, ASTM STP 1046, 1990, pp. 5-29.
- [13] R. K. Nanstad, K. Farrell, and D. N. Braski, *J. Nucl. Mater.* **158** (1988) 1.
- [14] K. Farrell, S. T. Mahmood, R. E. Stoller, and L. K. Mansur, *J. Nucl. Mater.* **210** (1994) 268.
- [15] L. K. Mansur and K. Farrell, "Mechanisms of Radiation-Induced Degradation of Reactor Vessel Materials," *J. Nucl. Mater.* (in press).
- [16] N. P. Baumann, Proceedings of the 7th ASTM-Euratom Symposium on Reactor Dosimetry, Strasbourg, France, 1990, pp. 689-97.
- [17] I. Remec, J. A. Wang, F.B.K. Kam, and K. Farrell, *J. Nucl. Mater.* **217** (1994) 258.
- [18] I. Remec and F.B.K. Kam, "Neutron Spectra at Different HFIR Pressure Vessel Surveillance Locations," NUREG/CR-6117, ORNL/TM-12484, Oak Ridge National Laboratory Report, Sept. 1993.
- [19] D. E. Alexander and L. E. Rehn, *J. Nucl. Mater.* **217** (1994) 213.
- [20] L. K. Mansur and H. Ullmaier, Proceedings of the International Workshop on Spallation Materials Technology, April 23-25, 1996, Oak Ridge, Tennessee, CONF-9604151.
- [21] J. O. Johnson, J. N. Barnes, L. A. Charlton, and T. A. Gabriel, Oak Ridge National Laboratory, private communication.
- [22] M. S. Wechsler, C. Lin, P. D. Ferguson, L. K. Mansur, and W. F. Sommer, "Calculations of Radiation Damage in Target, Container and Window Materials for Spallation Neutron Sources," Proceedings of the Second International Conference on Accelerator-Driven Transmutation Technologies and Applications, held in Kalmar, Sweden, on June 3-7, 1996, (in press).
- [23] E. H. Lee, N. H. Packan, M. B. Lewis, and L. K. Mansur, *Nucl. Inst. and Meth.* **B16** (1986) 251-259.